viruses

MDPI

Review

Dynamic Modeling of HIV-1 Gag Protein Transport, Polymerization and Assembly: A Differential Equation Perspective

Qianbin Tang [1,†], Jing Yang [1,†], Yan Peng [2] and Yuewu Liu [1,*]

[1] College of Information and Intelligence, Hunan Agricultural University, Changsha 410128, China
[2] College of Agronomy, Hunan Agricultural University, Changsha 410128, China
* Correspondence: yuewuliu@whu.edu.cn
† These authors contributed equally to this work.

Abstract

HIV-1 damages the human immune system and causes AIDS. It is a serious threat to human health and has become a major global public health issue. The Gag protein is a key structural protein of HIV-1. Dynamic models of Gag trafficking, polymerization and assembly can reveal the biophysical mechanisms of these processes. This can guide the development of highly effective anti-HIV-1 drugs and has practical value. This paper reviews three key stages of HIV-1 Gag prior to virus release using differential equation dynamics. First, Gag is produced near the nucleus. Molecular motors then transport it to the cell membrane. This process was mainly studied with convection–diffusion equation dynamic models. Second, Gag aggregates near the cell membrane into hexameric building blocks. This process mainly used ordinary differential equation dynamic models. Third, these building blocks assemble into immature HIV-1 virions. This step also mainly used ordinary differential equation dynamic models. Together, these mathematical models explained the biophysical principles of each process from a dynamic perspective. They can help biologists identify potential drug targets and develop effective anti-HIV-1 drugs.

Keywords: HIV-1 Gag; dynamics; mathematical model

1. Introduction

Human immunodeficiency virus type 1 (HIV-1) is a retrovirus that destroys the human immune system by preferentially attacking CD4 T lymphocytes, the central coordinators of the adaptive immune response [1]. Following entry into the host, HIV-1 infects these cells, integrates its proviral DNA into the host genome, and progressively depletes the CD4 T-cell population through direct cytopathic effects, chronic immune activation, and virus-mediated cell death [1]. As CD4 T lymphocyte counts steadily decline, the immune system gradually loses its capacity to mount effective responses against opportunistic infections and certain malignancies. This progressive and ultimately irreversible loss of immune function establishes HIV-1 as the principal pathogen responsible for acquired immunodeficiency syndrome (AIDS), the terminal clinical stage of HIV-1 infection. Accordingly, HIV-1 infection and AIDS remain among the most serious challenges to global public health.

According to the report released by the Joint United Nations Programme on HIV/AIDS (UNAIDS, https://www.unaids.org/en, accessed on 24 November 2026), the global HIV epidemic has exacted an enormous and enduring toll on human health and society. Since HIV-1 was first isolated in 1983 [2], an estimated 92.0 million people worldwide have been infected and some 44.2 million have died of AIDS-related illnesses. These figures underscore

Check for updates

Academic Editor: Nicholas C. Wu

Received: 14 October 2026
Revised: 24 November 2026
Accepted: 25 November 2026
Published: 27 November 2026

Copyright: © 2026 by the authors. Licensee MDPI, Basel, Switzerland. This article is an open access article distributed under the terms and conditions of the Creative Commons Attribution (CC BY) license.

both the scale of the epidemic and the considerable progress that has been made in diagnosis, treatment and prevention. In 2025, approximately 41.0 million people were living with HIV, including as many as 1.2 million new infections. This continued infection rate indicates that transmission has not yet been brought under control and that sustained prevention efforts remain indispensable. Encouragingly, approximately 32.1 million people were receiving antiretroviral therapy, reflecting a substantial expansion of treatment coverage that has markedly improved survival and quality of life for people living with HIV. Nevertheless, an estimated 570,000 people still died of AIDS-related illnesses in 2025 (UNAIDS, https://www.unaids.org/en, accessed on 24 November 2026). A sobering reminder that access to timely diagnosis, treatment and care remains unequal across regions and populations. Many infections are still detected too late. Indeed, the HIV-1 epidemic has been global in scope, reshaping public health systems, scientific research agendas, and societal responses. Collectively, these data highlight the urgent need for continued investment in prevention, testing, treatment, and the development of vaccines and curative strategies.

Assembly of Gag produces only immature, non-infectious particles. Their maturation into infectious virions requires proteolytic processing of Gag by the viral protease. Assembly is itself driven by Gag [3,4], a polyprotein that forms the principal structural framework of the virion. The precise timing and coordination of Gag–Gag interactions ultimately dictate the size, morphology, and infectivity of the released particle. During HIV-1 replication, Gag does not act as a static scaffold but instead undergoes a series of dynamic processes. Gag monomers are synthesized near the nuclear membrane [3]. Then they are transported by molecular motors from the cytoplasm to the plasma membrane [5]. Subsequently, the monomers oligomerize near the plasma membrane and further assemble into immature virions [3] (Figure 1). After budding from the host cell, the virion undergoes maturation, during which the viral protease cleaves Gag and Gag-Pol into their mature subunits and converts the immature particle into an infectious virion [3,4]. This sequence is highly ordered and spatiotemporally regulated, relying on both viral determinants and a range of host factors, such that perturbation of any step can reduce particle production or yield virions that are non-infectious [6,7].

From its N-terminus to its C-terminus, Gag consists of six domains: matrix (MA), capsid (CA), spacer peptide 1 (SP1), nucleocapsid (NC), spacer peptide 2 (SP2), and p6 [3,4,6,7,10]. These six domains perform distinct yet tightly integrated functions. MA directs Gag to the plasma membrane during early assembly and mediates Gag binding to the membrane [3]. This interaction is further stabilized by specific lipid determinants, namely PI(4,5)P_2, phosphatidylserine and cholesterol [4]. CA drives Gag–Gag polymerization through interactions between its N-terminal domain (NTD) and C-terminal domain (CTD), building the hexagonal lattice [6]. These lattices shape the immature HIV-1 particle. NC recognizes genomic RNA via the packaging signal and promotes RNA folding [6], thereby ensuring selective encapsidation of the viral genome. SP1 forms a multimerization core [4] and contributes the flexibility needed for proper lattice curvature. The p6 region contains the so-called late domain, which recruits the ESCRT machinery required for viral release [6]. Because each domain fulfils a discrete role while remaining functionally coupled to the others, the domain architecture of Gag provides the molecular basis for the stepwise progression from monomer transport, through polymerization, to membrane budding and, after proteolytic processing by the viral protease, to the formation of mature, infectious virions [3,4,6,7,10].

Gag is already a clinically validated antiviral target. Bevirimat, the first maturation inhibitor, blocks CA–SP1 cleavage and yields noninfectious particles with aberrant cores [11], a limitation was later addressed by BMS-955176, which had improved coverage for Gag polymorphisms [12]. Among CA binders, CAP-1 inhibits capsid assembly in vitro by

occupying a pocket in the N-terminal domain [13], whereas PF-74 acts at a distinct site and accelerates CA multimerization [14]. Structure-guided optimization produced lenacapavir, which binds the NTD–CTD interface with picomolar potency and, owing to slow release, maintains suppression with twice-yearly dosing [15].

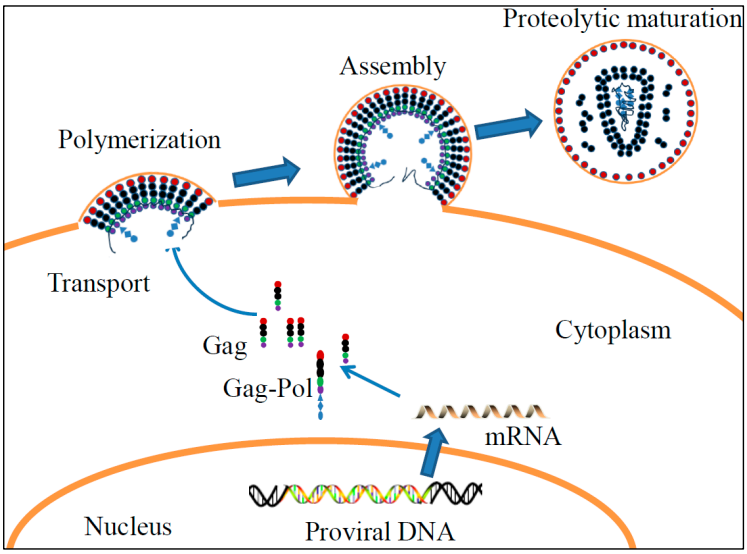


Figure 1. Schematic of HIV-1 Gag and Gag-Pol trafficking, polymerization and assembly, adapted from [8,9].

These Gag dynamic processes, spanning transport, polymerization and assembly, are inherently multiscale. They are therefore particularly well suited to mathematical and physical modeling, which can provide mechanistic insight into the processes underlying them and facilitate the development of highly effective anti-HIV drugs. Because viral assembly unfolds across multiple spatial and temporal scales, no single experimental technique can fully capture its complexity. Mathematical and physical modeling therefore offers a powerful complement to traditional biochemical and structural approaches [16–28]. Dynamic models can quantify the rates and equilibria of individual reaction steps, statistical-mechanical and coarse-grained models can describe the energetics of Gag–Gag and Gag–membrane interactions [29,30], and multiscale simulations can bridge molecular detail with mesoscopic and whole-cell behavior [31]. Such models make it possible to test hypotheses that are difficult to probe experimentally, to identify rate-limiting steps and sensitive parameters, and to predict how perturbations propagate through the assembly pathway.

From the perspective of differential-equation-based modelling, this review summarizes the kinetic and dynamic models of HIV-1 Gag that have been developed for the successive stages before virus release. Specifically, it is organized around the three processes emphasized in our title, including the transport of Gag from the site of synthesis to the plasma membrane, its polymerization into the immature lattice, and its subsequent assembly into immature virions. In doing so, this review aims to integrate dispersed modeling efforts into a coherent framework, to highlight the assumptions and limitations of current approaches, and to outline how improved models may guide the rational design of novel antiviral strategies targeting Gag-mediated assembly.

2. Dynamic Modeling of HIV-1 Gag Protein Transport

HIV-1 Gag is produced on cytosolic ribosomes as a soluble, myristoylated precursor [3,4]. Synthesized in the perinuclear region, it must subsequently be delivered to the plasma membrane, where new virions are assembled and released. This delivery is an active

process that depends on an intact microtubule network. Nonetheless, the identity of the molecular motors responsible for moving Gag remained unclear for many years. This gap was addressed by Martinez and colleagues, who identified KIF4 as one of the motors involved [5]. KIF4 is a kinesin that steps toward the plus end of microtubules. It binds Gag and propels the polyprotein outward along microtubules toward the cell periphery. When KIF4 was perturbed, Gag no longer passed through its successive transport intermediates in an orderly manner, and the yield of virus-like particles declined; re-introducing the motor restored normal behaviour. KIF4 also shields Gag from premature degradation, because depleting it accelerated Gag turnover and lowered intracellular Gag levels, an effect that re-expression of the motor could reverse. Under conditions of impaired KIF4 activity, Gag accumulated transiently in scattered perinuclear clusters. These clusters carried no endocytic markers, yet overlapped with KIF4, the SUMO-conjugating enzyme Ubc9, and SUMO itself, suggesting a previously unrecognized waystation on the path to assembly. Taken together, these findings cast KIF4 as a central regulator of both the intracellular journey and the lifetime of Gag, and highlighted motor-driven transport as an essential prerequisite for efficient Gag assembly [5].

Experimentally resolving such a spatially and temporally complex transport process is challenging, and this difficulty has motivated complementary theoretical treatments. A common strategy is to regard Gag transport as a convection–diffusion process, in which random diffusion is combined with directed, motor-driven movement. Liu et al. [17] adopted this viewpoint and formulated a convection–diffusion partial differential equation (PDE) model for Gag protein transport.

To make the problem tractable, they represented the cell as a sphere, thereby reducing the three-dimensional geometry to a one-dimensional problem along the radial direction without discarding the essential physics.

Here, treating the human CD4 T cell as a sphere is a reasonable approximation, because Stewart et al. [32] directly examined the cell geometry and showed that isolated cells are nearly spherical. A coordinate transformation was then applied to reduce the spherical domain, originally described in a three-dimensional Cartesian coordinate system, to a single radial dimension in spherical coordinates. This is purely a change in variables, and it leaves the models and the model predictions unchanged, although it substantially lowers the computational cost.

Under these assumptions, the model took the following form:

$$\frac{\partial P}{\partial t} = \frac{1}{r}\frac{\partial}{\partial r}\left(Dr\frac{\partial P}{\partial r} - srP\right) + g$$

where $\frac{\partial P}{\partial t}$ the partial derivative of P with respect to t. P denotes the concentration of Gag protein. D, s, and g are the diffusion coefficient, the convection coefficient, and the production rate, respectively. r and t denote the radial distance and time, respectively.

The three terms $(Dr\frac{\partial P}{\partial r}, srP, g)$ of the equation carry distinct biological meanings. Diffusion accounts for the random movement of Gag molecules from regions of higher concentration toward those of lower concentration. Convection represents the directed transport driven by molecular motors and the cytoskeleton. The production term captures the continuous synthesis of Gag precursor near the nucleus and its contribution to the local concentration. Together, these terms govern the spatiotemporal distribution of Gag along the radial axis, so that solving the equation allows one to predict how Gag concentration evolves over time and when it reaches the plasma membrane.

Because accurate solution of this model demands fine discretization in both space and time, the computational cost of a direct approach is substantial. To address this, Liu et al. [17] developed a parallel finite element algorithm. Parallel computation markedly raised the efficiency of solving the model, making it feasible to obtain numerical solutions

even on large discretized meshes. Using this framework, they estimated the time required for virus particle formation, which provided a basis for quantifying how the transport rate of Gag influences assembly and laid the foundation for coupling such transport models with polymerization and assembly models. Under the assumption that HIV-1 entry and egress occur on comparable timescales, the model of Liu et al. [17] predicted that virions appeared near the cell membrane at approximately twice the egress time, a prediction reported to agree principally with experimental data [33].

The convection–diffusion model of Liu et al. [17] represented an early kinetic description of Gag transport in the cytoplasm. Building upon it, Wang et al. [18] and Liu et al. [19] introduced polymerization kinetics near the plasma membrane, yielding more comprehensive integrated models that couple transport with polymerization. These models are discussed in detail in the section on dynamic models of Gag polymerization.

In the parameter sweeps of Liu et al. [17], the time required for virions to first appear at the plasma membrane scaled approximately inversely with microtubule transport speed, but was comparatively insensitive to the diffusion coefficient. Active transport, not diffusion, was therefore the rate-limiting step. This nominated the kinesin—Gag interaction as a candidate intervention point, consistent with KIF4 knockdown delaying Gag progression through its trafficking intermediates and reducing virus-like particle production [5]. However, it predicted arrival timing rather than virion yield. It also assumed quasi-monomers with no association or dissociation kinetics, and its parameters came from literature estimates rather than in-cell measurements.

3. Dynamic Modeling of HIV-1 Gag Protein Polymerization

3.1. In Vitro Versus In Vivo Differences in Gag Polymerization and Assembly

In vitro reconstitution with purified Gag defines the minimal requirements for assembly (protein concentration, ionic strength, nucleic acid scaffolding, and, for membrane-binding constructs, lipid composition) and provides controlled kinetic and structural data, whereas intracellular studies place the same reaction in its native context, linking polymerization to membrane targeting, trafficking, and particle release. The two approaches are complementary but not interchangeable [23,25].

In vitro, the reaction is closed, and its initial condition is set by the experimenter. Total Gag is fixed, and assembly is triggered by a controlled change in solution conditions (e.g., increased ionic strength or added nucleic acid). Because no external reservoir supplies or removes subunits, polymer increases monotonically as the monomer pool is depleted. The system, a closed-system mass-action process, is therefore defined solely by the initial monomer concentration, rate constants, and time [23,25].

In vivo, the reaction is open and spatially organized. Gag is synthesized in the cytosol and targeted to the inner leaflet of the plasma membrane, where MA-domain binding to acidic phospholipids raises the local concentration. The cytosolic pool acts as a reservoir that replenishes membrane monomers, so the local concentration is set by the balance of delivery, binding, and consumption, and products are likewise removed through budding, degradation, and proteolytic maturation. The intracellular reaction therefore has a source term, a finite and spatially heterogeneous monomer pool, and a product sink, all of which are absent from any closed in vitro assay [8,24].

These differences dictate model construction. A closed-system model conserves total Gag and needs only an initial monomer concentration, whereas an intracellular model must specify monomer influx from the cytosol, product efflux through assembly and release, and the coupling of three-dimensional cytosolic to two-dimensional membrane diffusion. In vitro kinetic parameters therefore cannot be transferred to the intracellular model without accounting for these sources and sink terms. The two regimes do, however, meet in

one limiting case. When monomer delivery to the membrane is fast relative to polymerization and product removal is slow relative to the observation window, the intracellular reaction approaches the constant-concentration, closed-system behavior of an in vitro assay. This limiting behavior provides a useful benchmark for validating the intracellular model.

3.2. Gag Polymerization In Vitro

Virus capsid assembly kinetics generally involve a lag period, a rapid assembly period, and an asymptotic period. These periods can be associated with particular, clearly defined characteristics of the reaction. The lag period is also called nucleation [34,35]. For HIV-1, Pornillos et al. [36,37] established approaches for purifying soluble CA hexamers that remain competent for assembly. They obtained four independent crystallographic models, defining the structure of this capsid assembly unit (building block) to atomic resolution. Therefore, HIV-1 nucleation ends with Gag hexamer polymerization [13–16].

Munoz-Alicea et al. firstly established nucleation polymerization model for HIV-1 [21]. The polymerization reactions are as follows:

$$\begin{aligned} &Gag_1 + Gag_i \underset{b_{1+i}}{\overset{f_{1i}}{\rightleftarrows}} Gag_{1+i}, i = 1, 2, \cdots, 5 \\ &Gag_2 + Gag_4 \overset{f_{24}}{\rightarrow} Gag_6, \\ &Gag_2 + Gag_2 + Gag_2 \overset{f_{22}}{\rightarrow} Gag_6, \\ &Gag_3 + Gag_3 \overset{f_{33}}{\rightarrow} Gag_6 \end{aligned}$$

where Gag_i is the polymer with i Gag monomers, f_{1j} is the value of the polymerization reaction, and b_{1+i} is the value of the dissociation reaction.

The simplified hexamer polymerization network adopted above omitted the association of two dimers, as well as the association between a dimer and a trimer. These reactions were omitted because their contribution was expected to be small, but they might partly have affected the predicted hexamer concentration.

Based on the mass conservation law and mass action law [28,38], Munoz-Alicea et al. [21] established ordinary differential equation (ODE) dynamical models:

$$\begin{cases} \frac{dc_1}{dt} = -2f_{11}c_{11}^2 - \sum_{i=2}^{5} f_{1i}c_1c_i + \sum_{i=2}^{5} b_ic_i \\ \frac{dc_2}{dt} = f_{11}c_{11}^2 + b_3c_3 - 3f_{22}c_2^3 - f_{24}c_2c_4 - f_{12}c_1c_2 - b_2c_2 \\ \frac{dc_3}{dt} = f_{12}c_1c_2 + b_4c_4 - f_{13}c_1c_3 - 2f_{33}c_3^2 - b_3c_3 \\ \frac{dc_4}{dt} = f_{13}c_1c_3 + b_5c_5 - f_{24}c_2c_4 - f_{14}c_1c_4 - b_4c_4 \\ \frac{dc_5}{dt} = f_{14}c_1c_4 - f_{15}c_1c_5 - b_5c_5 \\ \frac{dc_6}{dt} = f_{15}c_1c_5 + f_{22}c_2^3 + f_{24}c_2c_4 + f_{33}c_3^2 \end{cases}$$

where c_i (i = 1, 2,..., 6) is the concentration of the polymer with i Gag.

The listed polymerization reactions did not include two reactions: a dimer and a trimer polymerizing to a pentamer, and two dimers polymerizing to a tetramer. In addition, hexamers were considered stable polymers and not dissociated. This model addressed only the polymerization network, and no predictions were derived from it.

Based on the models presented by Munoz-Alicea et al. [21], Sadre-Marandi et al. [22] considered that two dimers polymerize to a tetramer.

$$Gag_2 + Gag_2 \underset{b_{22}}{\overset{f_{22}}{\rightleftarrows}} Gag_4$$

Moreover, they considered the dissociation reactions of all polymers.

Sadre-Marandi et al. [22] established a kinetic model for the chemical reactions by which the Gag protein polymerizes into hexamers in culture medium. Combined with experimental data, they used a particle swarm algorithm to estimate the values of the polymerization and dissociation coefficients of each chemical reaction. Through parameter sensitivity analysis, they inferred that the dimerization of two trimers to form a hexamer is the dominant reaction in the polymerization pathway. Moreover, sensitivity analysis of the model parameters indicated that CA dimers played a significant role during polymerization, in agreement with experimental findings [3]. However, they did not consider that a dimer and a trimer polymerize to a pentamer.

Sadre-Marandi et al. [22] used sensitivity and elasticity analysis to show that dimer formation and the trimer-of-dimers nucleation step provide greater leverage than the single-monomer addition pathway emphasized in earlier models, and further suggested that the most influential rate constants change over the course of nucleation, with early sensitivity dominated by association rates and later sensitivity shifting toward higher-order association rates. It should be noted that the fitted parameters were derived from in vitro assembly data for mutant CA protein, that no inhibitor or ligand binding was simulated, and that no validation was performed in cell-based or animal systems. The contribution of this study was therefore limited to providing a mechanistic basis for prioritizing targets rather than a validated antiviral strategy.

Based on the above models presented by Munoz-Alicea et al. and Sadre-Marandi et al., Liu et al. [23] considered the reduced hexamer polymerization reactions. The reactions are as follows.

$$Gag_i + Gag \underset{b_i}{\overset{f_i}{\rightleftarrows}} Gag_{i+1}, i = 1, 2, \cdots 5$$

where f_i is the value of the polymerization reaction, b_i is the value of the dissociation reaction.

They established a reduced polymerization kinetics model for the polymerization of the Gag protein into hexamers in vitro.

$$\begin{cases} \frac{dc_1}{dt} = -2f_1c_1^2 + 2b_1c_2 - \sum_{i=2}^{5} f_ic_1c_i + \sum_{i=2}^{5} b_ic_{i+1} \\ \frac{dc_i}{dt} = f_{i-1}c_1c_{i-1} + b_ic_{i+1} - b_{i-1}c_i - f_ic_1c_i, i = 2, 3, 4, 5 \\ \frac{dc_6}{dt} = f_5c_1c_5 - b_5c_6 \end{cases}$$

The initial condition is

$$c_1 = c_0, c_i = 0, i = 2, 3, 4, 5, 6.$$

The constraint condition is

$$\sum_{i=1}^{6} ic_i = c_0$$

where c_i (i = 1, 2,..., 6) is the concentration of the polymer with i Gag, and c_0 is the concentration of the monomer.

They carried out a systematic theoretical analysis and proved t.

They carried out a systematic theoretical analysis and proved the existence and uniqueness of the positive equilibrium point of the hexamer polymerization kinetics model. By means of the Routh—Hurwitz criterion, they determined that all the eigenvalues of the characteristic equation are negative, and thereby deduced that the model is locally asymptotically stable. This model was developed within an analytical framework only, and no quantitative predictions were derived from it.

The model of Liu et al. [23] yielded a rate-ratio logic, in which increasing the off-rate or decreasing the on-rate compressed the building-block pool, thereby providing semi-quantitative guidance for screening candidate molecules that disrupt protein—protein

contacts. It should be emphasized that these conclusions derived solely from qualitative analysis and analytical derivations of ordinary differential equation models.

In this subsection, all the polymerization reactions considered took place in vitro, where no newly added monomer concentration appeared, and hexamers were not consumed by participating in HIV-1 assembly. In the following subsection, we will review the polymerization in vivo.

3.3. Gag Polymerization In Vivo

Gag proteins, produced near the nucleus, are transported to the plasma membrane through the cytoplasm by molecular motor. Then they nucleated to the hexamers building blocks inside the plasma membrane. When these building blocks are accumulated to a critical concentration, the HIV-1 assembly starts.

Based on the polymerization of Gag in vivo, Liu et al. [24] considered a complete hexamer polymerization chemical reaction model for the Gag protein. Compared with the Gag protein polymerization reaction in vitro, the reaction in vivo involved a production rate of Gag protein monomers as well as a consumption rate of hexamers participating in viral particle assembly. Liu et al. [24] considered the polymerization reactions of HIV-1 Gag inside the plasma membrane as follows.

$$\begin{gathered}\phi \xrightarrow{\mu} Gag, \\ Gag_i + Gag \underset{b_i}{\overset{f_i}{\rightleftarrows}} Gag_{i+1}, i = 1, 2, \cdots 5 \\ Gag_6 \xrightarrow{r} assembly\end{gathered}$$

where μ denotes the production rate of Gag protein, r denotes the assembly rate of the hexamer, f_i is the value of the polymerization reaction, b_i is the value of the dissociation reaction.

The simplified hexamer assembly network assumed here allowed only one monomer to take part in each association step, and all other forms of association were treated as a sequence of single-monomer additions. This introduced a certain delay in the predicted change in hexamer concentration. This approximation affected the kinetics of hexamer formation rather than its equilibrium level.

Based on the models presented by Liu et al. [23], Liu et al. [24] established the dynamic model for HIV-1 Gag polymerization inside the plasma membrane as follows.

$$\begin{cases} \frac{dc_1}{dt} = -2f_1c_1^2 + 2b_1c_2 - \sum_{i=2}^{5} f_ic_1c_i + \sum_{i=2}^{5} b_ic_{i+1} + \mu \\ \frac{dc_i}{dt} = f_{i-1}c_1c_{i-1} + b_ic_{i+1} - b_{i-1}c_i - f_ic_1c_i, i = 2, 3, 4, 5 \\ \frac{dc_6}{dt} = f_5c_1c_5 - b_5c_6 - rc_6 \end{cases}$$

The initial condition is

$$c_1 = c_0, c_i = 0, i = 2, 3, 4, 5, 6.$$

They carried out a series of theoretical studies: they proved the existence and uniqueness of the positive equilibrium point of the hexamer polymerization reaction model in vivo, as well as its local asymptotic stability. This work was restricted to theoretical analysis, and no quantitative predictions were reported.

The model of Liu and Peng [24] yielded a corollary, namely that the steady-state building-block concentration was set by the monomer supply rate and the assembly consumption rate rather than by the association/dissociation rate constants. Inhibiting polymerization kinetics alone might therefore have been buffered by homeostasis, making

single-target intervention of limited efficacy, whereas reducing monomer supply or accelerating building-block consumption was theoretically more effective. It should be emphasized that these conclusions derived solely from qualitative analysis and analytical derivations of ordinary differential equation models.

3.4. Gag Transport in the Cytoplasm and Polymerization Inside the Plasma Membrane

While investigating the biological mechanism by which the Gag protein attaches to the cell membrane, Resh [34] found that the myristoylated matrix domain of Gag (myrMA) exists in two interconvertible switching states: an exposed state (myr-exposed, myr(e)) and a sequestered state (myr-sequestered, myr(s)). This transition is not random but is closely tied to the subcellular environment in which Gag resides, and it therefore constitutes a "myristoyl switch" that can be regulated by cellular signals. While Gag is being transported through the cytoplasm, myrMA is mainly in the sequestered state, in which the myristoyl group is buried within the protein and cannot readily associate with membrane lipids. Once Gag reaches the vicinity of the cell membrane, myrMA switches to the exposed state, in which the myristoyl group becomes extended and capable of inserting into the lipid bilayer. It is precisely this switching that allows Gag to bind the membrane at the correct time and location rather than attaching indiscriminately to membranous structures within the cytoplasm. Building on this, Resh [34] further found that the exposed myrMA forms an equilibrium between the monomer and the trimer $myrMA_3$. The polymerization reaction is as follows.

$$3myrMA \underset{k_{31}}{\overset{k_{13}}{\rightleftarrows}} myrMA_3$$

where k_{13} is the value of the polymerization reaction, and k_{31} is the value of the dissociation reaction.

On the basis of experimental observations, considering only the trimerization of myrMA as the mode of assembly is reasonable to a certain extent. However, the model allowed trimerization of only one Gag region, MA, and neglected CA–CA association, which was known to contribute to Gag lattice contacts and to the formation of CA hexamers and dimers. This omission rendered the model structurally incomplete.

Further taking into account the transport of the Gag protein through the cytoplasm, Wang et al. [18] sought to couple the two processes that had previously been treated separately: the directed movement of Gag toward the membrane and the myristoyl-switch—driven equilibrium between the myrMA monomer and trimer. To this end, they modified the convection–diffusion model of Liu et al. [17] by introducing its production-rate term, the combined rate of change arising from the synthesis and dissociation of the trimer. In this way, the original single-species transport equation was extended into a convection–diffusion–reaction equation model that describes how the monomer and trimer populations are transported, interconverted, and eventually bound at the cell membrane. The resulting model reads:

$$\begin{cases} \frac{\partial c_1}{\partial t} = \nabla \cdot (D\nabla c_1 - sc_1) + g - 3k_{13}{c_1}^3 + 3k_{31}c_3 \\ \frac{\partial c_3}{\partial t} = k_{13}{c_1}^3 - k_{31}c_3 - \gamma c_3 \end{cases}$$

where D, s, and g are the diffusion coefficient, the convection coefficient, and the production rate, respectively. c_1 and c_3 represent the concentrations of the myrMA monomer and trimer, respectively.

The reaction terms now explicitly captured the association of monomers into trimers and the dissociation of trimers back into monomers, so that the local balance between these two species was no longer imposed externally but emerged from the transport dynamics itself.

Because this coupled system was considerably more intricate than the single-equation model it generalizes, Wang et al. [18] analyzed the stability of the steady-state solution

and the existence of the positive solution. The model predicted that newly formed HIV-1 virions first appeared in the vicinity of the plasma membrane at approximately 10.1 h post-infection, in good agreement with the experimental observations [39]. At this time point, the concentrations of Gag monomers and trimers near the plasma membrane represent 2% and 98% of the total Gag pool, respectively. These results indicated that the present model could reproduce the experimental data [40].

Sensitivity analysis by Wang et al. [18] showed that the time at which new HIV-1 virions first appear near the cell membrane was governed mainly by the diffusion ratio and the transport ratio, and responded only weakly to the association efficiency. These results suggested that interfering with the microtubule-dependent intracellular trafficking of Gag might delay virion budding more effectively than perturbing the monomer–trimer association rate alone. These inferences remained theoretical, since no inhibitor or ligand binding was simulated and no validation was performed in cell-based or animal systems.

By combining gene knockout with site-directed mutagenesis, Kutluay and Bieniasz [35] dissected the initiating events of HIV-1 particle assembly and uncovered two distinct biological features of the Gag protein, one operating in the cytoplasm and the other at the plasma membrane. In the cytoplasm, while Gag monomers were being carried along microtubules, only a small fraction of them associated into dimers. Importantly, no species of higher order than the dimer could be detected under these conditions. This observation suggested that cytoplasmic Gag multimerization was deliberately restricted, so that the protein did not prematurely assemble into large structures before reaching its destination. Therefore, the dimer appeared in the cytoplasm, the only oligomeric intermediate on the assembly pathway. Its formation was governed by the following polymerization reaction:

$$
\begin{aligned}
2Gag &\underset{k_1'}{\overset{k_1}{\rightleftarrows}} Gag_2,\\
\phi &\xrightarrow{g} Gag,\\
Gag &\xrightarrow{d_1} \phi,\\
Gag_2 &\xrightarrow{d_2} \phi.
\end{aligned}
$$

where the second reaction describes the production of Gag monomer, and the last two reactions describe the degradation of Gag monomer and dimer.

Near the cell membrane, the situation changed markedly. Once Gag had been delivered to the site of particle formation, further subunit–subunit contacts were permitted. Gag protein began to polymerize in an ordered stepwise manner. Rather than elongating through arbitrary intermediates, this process proceeded toward the building-block hexamer, which served as the fundamental unit from which the higher-order lattice of the immature virion was subsequently constructed. This stepwise conversion of membrane-associated Gag into hexamers was described by the following polymerization reaction:

$$
\begin{aligned}
Gag_i + Gag_j &\underset{k_{ij}'}{\overset{k_{ij}}{\rightleftarrows}} Gag_{i+j}, i \le j, i+j \le 6, i, j = 1, 2, \cdots 6\\
Gag_n &\xrightarrow{d_n} \phi, n = 1, 2, \cdots, 6
\end{aligned}
$$

where the last reaction describes the degradation of the polymer withconvection–diffusionGag monomers.

Here, all chemical reactions describing dimer association in the cytoplasm and hexamer formation at the plasma membrane were constructed separately on the basis of experimental data. The most complete reactions were considered here. Oligomers larger than the hexamer have not been detected experimentally, possibly because their concentrations are low. If

such species do form, they would consume part of the hexamer pool and thus slightly reduce the hexamer concentration.

Based on the above polymerization reaction, Liu et al. [19] constructed a more comprehensive model of Gag transport and polymerization kinetics, taking the convection–diffusion framework of Liu et al. [17] as its point of departure.

In the cytoplasm, the guiding principle of their approach was to preserve the transport description of Gag monomers within the cytoplasm while simultaneously embedding it in a reaction network that mirrors the successive oligomerization events observed experimentally. To this end, they appended to the convection–diffusion equation for cytoplasmic monomers a chemical reaction term that captures the reversible association between the monomer and the dimer. The coupled system therefore connected cytoplasmic trafficking to the very first step of polymerization:

$$\begin{cases} \frac{\partial c_1}{\partial t} = \frac{1}{r}\frac{\partial}{\partial r}\left(D_1 r \frac{\partial c_1}{\partial r} - s_1 r c_1\right) + g + 2k'_1 c_2 - 2k_1 c_1^2 - d_1 c_1 \\ \frac{\partial c_2}{\partial t} = \frac{1}{r}\frac{\partial}{\partial r}\left(D_2 r \frac{\partial c_2}{\partial r} - s_2 r c_2\right) + k_1 c_1^2 - k'_1 c_2 - d_2 c_2 \end{cases}$$

At the plasma membrane, which in the model corresponds to the domain boundary, they further incorporated a chemical reaction term governing the stepwise polymerization of Gag monomers into the hexamer. The complete formulation is given in the original work of Liu et al. [19] as follows.

$$\begin{cases} \frac{\partial c_1}{\partial t} = \frac{1}{r}\frac{\partial}{\partial r}\left(k_D D_1 r \frac{\partial c_1}{\partial r} - k_s s_1 r c_1\right) + 2k'_1 c_2 - 2k_1 c_1^2 + \sum_{i=2}^{5}(k'_{1i} c_i - k_{1i} c_1 c_i) - d_1 c_1 \\ \frac{\partial c_2}{\partial t} = \frac{1}{r}\frac{\partial}{\partial r}\left(k_D D_2 r \frac{\partial c_2}{\partial r} - k_s s_2 r c_2\right) + k_{11} c_1^2 - k'_{11} c_2 + \sum_{i+j\le 6}\left(k'_{ij} c_{i+j} - k_{ij} c_i c_j\right) - d_2 c_2 \\ \frac{\partial c_m}{\partial t} = \sum_{i+j=m}\left(k_{ij} c_i c_j - k'_{ij} c_m\right) + \sum_{i+m\le 6}(k'_{im} c_{i+m} - k_{im} c_i c_m) - d_m c_m, m = 3,4,5,6 \end{cases}$$

By quantifying the relative contributions and weights of all the pathways that can give rise to the hexamer, Liu et al. [19] singled out the principal routes of hexamer synthesis: the joining of two Gag monomers to form a dimer, the combination of a monomer with a dimer to yield a trimer, and the union of two trimers to generate a hexamer. The principal polymerization reactions of hexamer synthesis are as follows.

$$\begin{aligned} &Gag + Gag \rightleftarrows Gag_2, \\ &Gag + Gag_2 \rightleftarrows Gag_3, \\ &Gag_3 + Gag_3 \rightleftarrows Gag_6. \end{aligned}$$

From this pathway analysis they further concluded that the dimer and the trimer act as the two pivotal intermediates in the assembly of the hexamer, in agreement with experimental findings [36]. In addition, by simulating combination-drug experiments in which Gag synthesis is suppressed, they identified the N-terminal glycine residue of the MA region of the Gag protein as a promising drug target, in agreement with experimental findings [34,39].

Liu and Zou [19] inferred from their model that the dimer and the trimer are key intermediates in hexamer formation. The early dimer and trimer nodes were quantitatively more important than the later polymerization steps, so an inhibitor acting there did not need to achieve a high inhibition efficiency to cause a substantial reduction in hexamer. The trimer was also a sensible intervention node on biological grounds, since its formation marked the point at which the complex was anchored to the membrane. Blocking dimerization or trimerization therefore interrupted assembly before the virus began to grow. The authors further simulated four theoretical combined suppression strategies and, together with the fit to the MA N-terminal glycine mutant (G2A), proposed that this residue is a promising drug target. Both lines of argument remained theoretical, as no compound or ligand was simulated and no validation was performed in cells or animals.

4. Dynamic Modeling of HIV-1 Gag Protein Assembly

4.1. Gag Assembly In Vitro

Stephen and Alan [41] examined the assembly properties of purified, recombinant HIV-1 Gag protein by using an in vitro assembly system. They also studied the assembly properties of Gag missing the C-terminal p6 domain (Gag Δp6). They firstly synthesized HIV virus-like particles (VLP) from Gag protein in vitro. These virus particles had a radius of 25–30 nm, and the distance between the centers of adjacent Gag hexamers was 5–7 nm.

Liu et al. [25] simplified the assembly process of HIV VLP. Only one hexamer building block participated in each assembly step, and the simplified assembly chemical reaction was as follows:

$$\begin{gathered} H + H \underset{k_1^-}{\overset{k_1^+}{\rightleftarrows}} H_2 \\ H_2 + H \underset{k_2^-}{\overset{k_2^+}{\rightleftarrows}} H_3 \\ \vdots \\ H_{N-1} + H \underset{k_{N-1}^-}{\overset{k_{N-1}^+}{\rightleftarrows}} H_N \end{gathered}$$

where H_i denotes the intermediate of the HIV virus-like particle possessing i hexamer building blocks.

Here, each assembly step was assumed to involve a single building block, the hexamer. Because a VLP comprised nearly one hundred such blocks, its assembly was highly complex, and steps in which several blocks associated at once were therefore represented as a series of sequential single-block additions. This simplification was reasonable to a certain extent, in that it altered the kinetics of VLP assembly but not the extent of assembly reached at equilibrium.

Based on the above simplified assembly process of HIV VLP, Liu et al. [23] established an assembly kinetics model:

$$\begin{cases} \frac{d[H]}{dt} = -\left(2k_1^+[H]^2 + k_2^+[H][H_2] + \cdots + k_{N-1}^+[H][H_{N-1}]\right) \\ \qquad\quad +\left(2k_1^-[H_2] + k_2^-[H_3] + \cdots + k_{N-1}^-[H_N]\right) \\ \frac{d[H_2]}{dt} = k_1^+[H]^2 - k_2^+[H][H_2] + k_2^-[H_3] - k_1^-[H_2] \\ \qquad \vdots \\ \frac{d[H_{N-1}]}{dt} = k_{N-2}^+[H][H_{N-2}] - k_{N-1}^+[H][H_{N-1}] + k_{N-1}^-[H_N] - k_{N-2}^-[H_{N-1}] \\ \frac{d[H_N]}{dt} = k_{N-1}^+[H][H_{N-1}] - k_{N-1}^-[H_N] \end{cases}$$

where $[H_i]$ is the intermediate concentration of the HIV virus-like particle possessing i hexamer building blocks.

The initial condition is

$$[H] = C_0, [H_i] = 0, i = 2, 3, \cdots, N.$$

The constraint condition is

$$\sum_{i=1}^{N} i[H_i] = C_0$$

Liu et al. [25] carried out a mathematical theoretical analysis of the above large-scale assembly kinetics model. They proved the existence and uniqueness of the positive equilibrium point of these models. Then they theoretically analyzed the relationships, in the equilibrium state, between the concentrations of all intermediates and the macroscopic polymerization coefficients and the size of the nucleus structure. They also gave upper and lower bounds for the concentration of HIV VLP in the equilibrium state. This model addressed only the polymerization network, and no predictions were derived from it.

Liu and Zou [25] proved by theoretical analysis that an intervention lowering only the association rates, while leaving the intersubunit contact energetics intact, could merely delay the approach to equilibrium. Such an intervention could not alter the equilibrium distribution of intermediates or of completed particles. Lowering the final yield instead required a change in the association constant set by the contact free energy, or a reduction in the effective concentration of free building blocks. These conclusions remained far from the development of an anti-HIV-1 therapeutic, but they sharpened our understanding of the assembly dynamics of HIV-like particles in vitro.

4.2. Gag Assembly Inside the Plasma Membrane

The above is the assembly situation of the Gag protein in vitro. The following reviews the more complex assembly situation within the host cell. The Gag protein is the major structural protein of the immature HIV-1 particle; these proteins accumulate on the inner side of the host plasma membrane and gradually form spherical virus particles with a radius of about 130 nm, requiring about 2500 Gag protein monomers (about 420 Gag hexamer building blocks) [3,4,10].

Based on the above assembly process of immature HIV-1 particles within the host cell, Liu et al. [8] added a production-rate term for the Gag hexamer to the first equation of the assembly kinetics model established by Liu et al. [25] for culture medium. Furthermore, they added a release-rate term for the final assembled form (the immature HIV-1 particle) to the last equation. The constraint of the Gag protein concentration was removed. At the same time, in the assembly chemical reactions, they considered the polymerization of multiple Gag hexamer building blocks at once. The reduced assembly reactions were as follows.

$$\begin{gathered}
\phi \xrightarrow{g} H \\
H + H_6 \underset{k_7^-}{\overset{k_7^+}{\rightleftarrows}} H_7 \\
H_7 + H_6 \underset{k_{13}^-}{\overset{k_{13}^+}{\rightleftarrows}} H_{13} \\
\vdots \\
H_{N-6} + H_6 \underset{k_N^-}{\overset{k_N^+}{\rightleftarrows}} H_N \\
H_N \xrightarrow{r} release
\end{gathered}$$

where the first reaction describes the production of hexamer, the last reaction describes the release of immature HIV-1.

In vivo, a VLP contained 420 building blocks, and on average about 30 blocks lied along the exposed edge of each assembly intermediate. It was therefore more reasonable to let six blocks associate at each step than to retain the single block per step assumption used in vitro. The same limitation nevertheless applied, in that more than six blocks might associate simultaneously. This simplification altered the kinetics of VLP assembly but not the extent of assembly reached at equilibrium.

Moreover, they established a functional relationship for the association and dissociation coefficients through the statistical factor values of the polymerization intermediates. The function in [8] is as follows.

$$k_i^+ = fS_i, k_i^- = fa_i K_{Acon}^{-c_i}, K_{Acon} = e^{-\Delta G_c/RT}$$

where ΔG_c is the free energy, R is the gas constant, T is the temperature in Kelvin, and S_i, c_i, a_i are the statistical factors of intermediates.

The reduced dynamic model presented by Liu et al. [8] was as follows.

$$\begin{cases} \frac{d[H]}{dt} = -\left(7k_7^+[H]^7 + 6k_{13}^+[H]^6[H_7] + \cdots + 6k_N^+[H]^6[H_{N-6}]\right) \\ \qquad\qquad +\left(7k_7^-[H_7] + 6k_{13}^-[H_{13}] + \cdots + 6k_N^-[H_N]\right) + v \\ \frac{d[H_7]}{dt} = k_7^+[H]^7 - k_{13}^+[H]^6[H_7] + k_{13}^-[H_{13}] - k_7^-[H_7] \\ \qquad\vdots \\ \frac{d[H_{N-6}]}{dt} = k_{N-6}^+[H]^6[H_{N-12}] - k_N^+[H]^6[H_{N-6}] + k_N^-[H_N] - k_{N-6}^-[H_{N-6}] \\ \frac{d[H_N]}{dt} = k_N^+[H]^6[H_{N-6}] - k_N^-[H_N] - r[H_N] \end{cases}$$

where v in the first equation is the production rate of hexamer building blocks, and r in the last equation is the value of immature HIV-1 particle release.

By simplifying the chemical reaction equations and establishing the functional relationship between the parameters, the number of parameters was reduced by half to avoid over-fitting in parameter optimization.

Liu et al. [8] carried out a mathematical theoretical analysis of the assembly kinetics model of immature HIV-1 particles within the host cell. They proved the existence and uniqueness of the positive equilibrium point of the assembly kinetics model. They analyzed the relationship, in the equilibrium state, between the concentration of immature HIV-1 particles and the macroscopic polymerization coefficients.

Based on biological experimental data, they estimated the size of the nucleation intermediate during the assembly process by means of the assembly kinetics model. At the same time, they found that the macroscopic polymerization coefficient for forming the nucleus intermediate was far smaller than the subsequent macroscopic polymerization coefficients. This finding explained the kinetic mechanism by which efficient assembly began only after the free hexamer building blocks had accumulated to a certain concentration.

The number of puncta (i.e., small, discrete fluorescent spots or particle clusters in microscopy) was simulated over a 40-min window at 5–6 h after transfection. The simulated puncta count at 17 time points was consistent with the experimental data [42].

Liu and Zou [8] showed by theoretical analysis that, at equilibrium, the concentration of completed capsids was set by the production and release fluxes rather than by the association rates. This result implied that target selection should have shifted away from the polymerization step. An inhibitor that only slowed hexamer association pushes the population toward free subunits without reducing the final yield. Lowering that yield instead required acting on the supply of building blocks. These inferences remained theoretical, with no simulated inhibitor binding and no cellular or animal validation.

The models reviewed in this section, like those in the preceding two sections, rest on parameters that are estimated rather than measured directly. To provide a balanced assessment of the reviewed approaches, the following section examines how these parameters are determined and how uncertainty in them influences the reliability of the predictions discussed above.

5. Parameter Estimation

The models surveyed in Sections 2–4 differ not only in mathematical structure but also in how their parameters are assigned. Because the accuracy and biological relevance of a kinetic model depend on parameter estimation, this section compares how the key kinetic parameters are determined and how uncertainty in them affects the predicted assembly dynamics.

Two attitudes toward parameterization coexist in the literature. A number of transport, polymerization and assembly models were constructed as analytical frameworks in which no formal fitting is reported. Liu et al. [17], Munoz-Alicea [21], Liu et al. [23,24] and Liu and

Zou [25] left the diffusion and convection coefficients, the production and consumption rates, and the association and dissociation coefficients undetermined. These models derived only qualitative results. Such results concerned the existence, uniqueness and local asymptotic stability of the positive equilibrium, or upper and lower bounds on the virion concentration. They held for any parameter values that satisfy the stated constraints.

The second attitude is to estimate parameters from measured data. Three strategies appear in the reviewed work.

The first is the Tikhonov regularization method [43]. A penalty proportional to the magnitude of the parameters is added to the least-squares objective, which keeps the estimate stable when the data are noisy and the parameters are only weakly identifiable. This method has been adopted by Liu and Zou [19], Sadre-Marandi et al. [22], and Liu and Zou [8]. The general form is as follows.

$$\min J(\theta) = \left\| Y(\theta) - Y^{(\exp)} \right\|_2 + \lambda \|\theta\|_2$$

where the first term represents the error between the calculated results and the experimentally observed values, and the second term is the Tikhonov regularization term.

The second is the particle swarm optimization algorithm, in which a population of candidate parameters is iteratively moved toward the best-fitting parameters of that population. Sadre-Marandi et al. [22] applied this method to concentration data spanning Gag monomers to hexamers and estimated the polymerization and dissociation coefficients of each reaction. Liu and Zou [19] also applied this method to monomer-to-hexamer Gag concentrations measured in both wild-type and mutant settings, and the polymerization and dissociation coefficients were identified.

The third is an approach that establishes a functional relationship between the association and dissociation rate constants using statistical factors, thereby reducing the number of parameters. By adopting this method, Liu and Zou [8] reduced the number of parameters by half, thereby effectively mitigating overfitting. The function used in their work is given below.

$$k_i^+ = \frac{S_i}{a_i K_{Acon}^{-c_i}} k_i^-$$

where k_i^+, k_i^- are the association and dissociation rate constants, S_i,a_i,c_i are statistical factors, and K_{Acon} is a constant.

6. Conclusions and Outlook

To place the contributions summarized above in a broader perspective, Table 1 collates the representative differential-equation models of HIV-1 Gag transport, polymerization and assembly. We compare these models along six dimensions: the biological stage and system represented, the mathematical framework and its underlying assumptions, the parameter estimation and analysis performed, the principal predictions reported, the experimental evidence invoked in support, and the main limitations acknowledged. Read as a whole, the comparison reveals a clear division in the existing literature. PDE-based models have been used almost exclusively to describe cytoplasmic transport in spherical-cell geometries. ODE-based models, by contrast, have addressed polymerization and assembly on the inner side of the cell membrane. This division is convenient, and it is the reason the field has advanced stage by stage. Beyond the differential-equation treatments collected in Table 1, other researchers have proposed kinetic and simulation models of the same three processes. For example, Ayton and Voth [29] studied a coarse-grained method for the assembly of immature HIV-1 particles, and Grime et al. [30] developed a coarse-grained method for the assembly of mature HIV-1 particles. These are not reviewed one by one here.

Table 1. Comparative summary of representative differential-equation models of HIV-1 Gag transport, polymerization and assembly.

Model	Biological Stage/System	Mathematical Framework and Key Assumptions	Parameter Estimation and Analysis	Main Predictions/Findings	Experimental Support	Main Limitations
Liu et al. (2012) [17]	Monomer transport, cytoplasm	Convection–diffusion PDE; spherical cell	Parallel finite-element algorithm; no parameter fitting reported	Spatiotemporal Gag distribution, VLP-formation time; an early kinetic framework	KIF4-motor transport [5]	Transport only; no parameter fitting
Wang et al. (2015) [18]	Monomer transport, cytoplasm; MyrMA polymerization, membrane	Convection–diffusion–reaction PDEs; spherical cell	Steady-state analysis; no parameter fitting reported	Steady-state analysis; VLP-formation time	Myristoyl-switch mechanism [34]	No high-order polymerization
Liu and Zou (2017) [19]	Dimer polymerization and transport, cytoplasm; hexamer polymerization, membrane	Convection–diffusion–reaction PDE for cytoplasmic, ODE for membrane; spherical cell	Tikhonov regularization method; sensitivity analysis; identifiability analysis	Monomer–dimer and trimer–trimer routes as principal pathways; dimer and trimer as key intermediates; MA N-terminal glycine as candidate target	Cytoplasmic dimer only [35]; hexamer building block [35–37]	No high-order polymerization
Munoz-Alicea (2013) [21]	Monomer transport, cytoplasm; hexamer polymerization, membrane	Convection–diffusion PDE, ODE; spherical cell	Parallel finite-element algorithm; no parameter fitting reported	Spatiotemporal Gag distribution; VLP-formation time; early kinetic framework for hexamer nucleation	KIF4-motor transport [5], hexamer building block [35–37]	Separate modeling of transport and polymerization
Sadre-Marandi et al. (2015) [22]	Hexamer polymerization, in vitro	ODE; nucleation and elongation	Particle-swarm optimization; sensitivity analysis	Identify importance of CA in the nucleation stage	Concentrations of monomer to hexamer [36,37]	No transport
Liu et al. (2022) [23]	Hexamer polymerization, in vitro	ODE; one monomer added per step	Steady-state analysis; no parameter fitting reported	Positive equilibrium point existed and was unique; was locally asymptotic stable	Hexamer building block [35–37]	Reduced reactions; no parameter fitting
Liu and Peng (2024) [24]	Hexamer polymerization, in vivo	ODE; one monomer added per step; monomer production and hexamer consumption	Steady-state analysis; no parameter fitting reported	Positive equilibrium point exists and is unique; locally asymptotic stable	Hexamer building block [35–37]	Reduced reactions; no parameter fitting
Liu and Zou (2017) [25]	VLP assembly, in vitro	ODE; one hexamer added per step	Steady-state analysis; upper and lower bounds	Relate intermediate concentrations to macroscopic coefficients and nucleus size; bounds virion concentration	In vitro VLP size and hexamer spacing [41]	One hexamer addition; no parameter fitting
Liu and Zou (2019) [8]	Intracellular immature HIV-1 assembly	ODE; multiple-hexamer addition; virion release	Steady-state analysis; nucleus-size estimation	Nucleus-formation coefficient much smaller than subsequent coefficients; explain threshold-like assembly	Intracellular particle size and Gag number [49]	No transport; no explicit budding mechanics

This review is concerned with Gag transport, polymerization and assembly; that is, with the events leading to the formation and release of the immature, budded particle. HIV-1 maturation is a temporally and mechanistically distinct post-budding stage, in which the activated viral protease cleaves Gag and the spherical immature lattice is converted into the conical capsid. How the immature lattice is converted into the cone remains under active investigation. Some studies support disassembly of the immature lattice followed by de novo reassembly [44], whereas others describe a non-diffusional, displacive phase transition of the existing lattice [45]. Later evidence indicates that the two processes act in sequence rather than in competition [46]. Both the measurement of protease activity [47] and the potential drug targets proposed at the Gag and protease interface [48] are topics of considerable current interest. HIV-1 maturation is thus both a focus of intense study and a persistent technical challenge, yet it lies outside the scope of this review and is therefore not discussed here in detail.

6.1. Gag Transport, Polymerization and Assembly: A Continuous Process

In the infected cell Gag transport, polymerization and assembly overlap in space and time, and each one sets the initial condition for the next. Transport determines when and where the membrane-proximal Gag concentration becomes sufficient for nucleation. Polymerization converts that supply into hexameric building blocks, and the accumulation of these blocks past a critical level is what allows assembly to begin. Assembly, in turn, removes hexamers from the membrane and releases completed particles, which lowers the local concentration and reshapes the gradient that drives transport. The literature reviewed above contains all three couplings, but it contains them implicitly, embedded in models that were built to describe one stage and were later extended to accommodate a second. A comprehensive model should incorporate all three processes.

Supply-limited initiation. Transport sets the arrival flux and therefore the time at which polymerization becomes favorable. The quantitative consequences are large. The transport-only model of Liu et al. [17] placed the appearance of virions near the membrane at approximately twice the egress time. When the same transport description was coupled to the myristoyl-switch equilibrium, Wang et al. [18] predicted first appearance at about 10.1 h post-infection, in agreement with live-cell imaging. The coupled model further predicted that at this time point the membrane-proximal population of Gag was 2% monomer and 98% trimer, which showed that the effective substrate for polymerization was not the total Gag concentration but the fraction that the switch had converted into the assembly-competent state.

Spatial gating by the myristoyl switch. Transport delivers Gag in the sequestered state, and proximity to the membrane converts it to the exposed state [35]. The switch therefore does more than regulate a rate. It selects the location at which polymerization may begin, and it prevents the premature oligomerization that Kutluay and Bieniasz [36] showed to be suppressed in the cytoplasm, where the dimer is the only oligomeric species detected.

Downstream feedback. Polymerization and assembly consume monomer and hexamer, so they act as a membrane-localized sink. Liu and Peng [24] represented this as a hexamer consumption rate, and Liu and Zou [8] represented it as a release rate for the completed particle. These two quantities were exactly what a transport model should have supplied at its boundary and what a polymerization model should have consumed at its source. In the current formulations they were held constant, which severed the loop. A spatially resolved treatment would let the sink depress the near-membrane concentration, steepen the cytoplasmic gradient, and thereby feedback on transport itself.

6.2. Challenges Facing an Integrated Model

Scale mismatch. Transport takes place over hours and across the entire cell, whereas the generation of building blocks and the assembly of virus particles take place over minutes and across tens of nanometers. Liu et al. [19] addressed transport within the cytoplasm and the polymerization kinetics of building blocks at the cell membrane, but did not consider the assembly of virus particles in subsequent stages.

Failure of the well-mixed assumption at the budding virion. Every ODE model reviewed here treats the inner leaflet as a homogeneous compartment. An immature particle of 130 nm radius carrying about 420 hexamers is not well mixed on the relevant timescale. Once the bud exceeds a few tens of nanometers, the local hexamer concentration at its rim differs from that on the surrounding membrane, and a compartmental description can no longer represent the competition between neighboring budding sites. Resolving this requires reaction-diffusion on a curved surface or particle-based lattice kinetics.

Parameter proliferation and identifiability. Each stage brings its own rate constants, and most of them cannot be measured in vivo. Two existing strategies point the way forward. Liu et al. [19] used Tikhonov regularization together with sensitivity and identifiability analysis, and Liu and Zou [8,19] used statistical factors together with a free-energy relation to halve the parameter count. A three-stage model multiplies the unknowns further, and it will require hierarchical or Bayesian estimation, global sensitivity analysis, and explicit model selection rather than point fitting.

Small-number effects near nucleation. The nucleus-size estimates of Liu and Zou [8], together with the lag-phase analysis of Hagan and Elrad [28], indicate that the critical nucleus is small. When the number of hexamers per budding site is small, deterministic rate equations describe an average that no individual site follows. A stochastic or hybrid treatment is needed if the model is to reproduce the site-to-site variability visible in live-cell recordings.

Unmodelled molecular actors. The transport models treat Gag as passive cargo carried by KIF4 [5], with no role for the perinuclear clusters, for cortical actin, or for the membrane composition that Gag itself alters. The polymerization models omit genomic RNA. This is a notable simplification, because in vivo the genomic RNA is packaged by NC, and this RNA–protein complex is believed to act as a scaffold that templates lattice formation and lowers the effective nucleation barrier.

Validation. Current models are checked against bulk biochemical time courses or against puncta counts. An integrated model makes simultaneous predictions about arrival flux, hexamer kinetics, bud size distribution, and particle yield, and it should be constrained by all of them at once.

6.3. Open Problems Requiring Further Study

(1) Why does the immature particle stop growing at a radius of about 130 nm [3]? Every assembly model in Table 1 treats the final size as an input rather than an output. Liu and Zou [8] fixed the completed particle at about 420 hexamer building blocks, and Liu and Zou [25] terminated the intermediate chain at the size observed in vitro. These models therefore reproduced the measured radius, but they did not explain why growth ceased there. The question is sharpened by the fact that the free energy of adding a hexamer to a flat lattice face remains favorable well beyond 130 nm, so closure must have a geometric or mechanical origin. Dharmavaram et al. [32] proposed the concept of a geometric potential energy barrier, arguing that this energy arises from the interaction between the positive Gaussian curvature of the particle surface and the negative Gaussian curvature of the particle neck, and the concept was derived within Helfrich elastic theory. Whether such a barrier can be embedded in a lattice-kinetic or

reaction-diffusion treatment, and whether it accounts quantitatively for the observed distribution of particle sizes rather than for a single radius, still requires further study.

(2) The transition of the virus particle from immature to mature. In this process the protease cleaves the MA region and the CA domain of the Gag protein, and the CA domain then forms the conical capsid. Cleavage is irreversible, and it changes the stoichiometry, so the equilibrium and path-independence arguments used to justify the simplified reaction networks do not carry over.

(3) By what biophysical principle does Gag supply the energy for budding? As Gag polymerizes on the inner side of the host membrane, the bud grows outward against the bending rigidity of the bilayer. The models reviewed here treated this growth as a release rate, which was fitted rather than derived from the mechanics of the lattice. What remains unclear is how the free energy released by lattice formation is partitioned between the elasticity of the Gag shell, the bending and stretching of the membrane, and the ESCRT-mediated scission event. Answering this question requires the same ingredient that problem (1) requires, namely a coupling between the kinetic description and membrane mechanics.

6.4. Opportunities

A modular coupling architecture. The modules already share interface variables, namely the membrane arrival flux, the membrane-proximal monomer and trimer concentrations, the hexamer concentration, and the release rate. An integrated model can therefore be assembled by coupling validated modules through explicit interface conditions, rather than by re-deriving a single monolithic model. This preserves the assumptions under which each module was tested and makes the coupling itself testable.

A single free-energy scale. The statistical-factor formulation used by Liu and Zou [8,19], following Zlotnick [27], already ties association and dissociation coefficients to a free-energy difference. The same device can be extended to membrane insertion and to myrMA trimerization, so that the myristoyl-switch equilibrium, the hexamer association constants, and the lattice contact energies are all expressed on one thermodynamic scale. This would reduce the parameter count and would guarantee that an integrated model does not violate detailed balance across stages.

Linking kinetics to membrane mechanics. Problems (1) and (3) in Section 6.3 both require a mechanical description of the particle and the surrounding bilayer, and the Helfrich framework invoked by Dharmavaram et al. [32] is the natural candidate. A kinetic model with a curvature-dependent rate for hexamer addition would let particle size become a prediction rather than an input, and it would connect the kinetic and structural literature that are currently separate.

Distinguishing stage-specific from pathway-wide targets. An integrated model propagates a perturbation from the stage where it acts to the stages downstream. The models reviewed here have already nominated targets at each stage: the myristoyl switch [18], the N-terminal glycine of MA [19], CA–CA contacts [21], and the trimer–trimer route to the hexamer [18,19]. What is not yet available is a comparison of their relative leverage. A coupled model would show whether inhibiting transport and inhibiting nucleation differ in the shape of the resulting dose–response curve, and it would allow combination-drug experiments to be simulated before they are performed.

Testable predictions and designed experiments. The threshold-like onset reported by Liu and Zou [8], in which the macroscopic coefficient for forming the nucleus was far smaller than the subsequent coefficients, predicted a steep dependence of particle number on Gag supply. Coupling this to transport predicted whether nucleation or delivery was

rate-limiting as a function of expression level, which was directly testable by titrating Gag expression, by depleting KIF4, and by measuring the lag before the first particle appeared.

Data and standards. Live-cell quantitative imaging, single-molecule tracking, fluorescence recovery after photobleaching and cryo-electron tomography of budding sites now provide the constraints that an integrated model needs. For the models themselves, distribution in a standard exchange format with explicit units would let modules be composed and compared, which is a precondition for the kind of integration the field now requires. Structural biology studies of HIV-1 Gag protein provide microscopic-level information about Gag, including its electrostatic properties, spatial geometry, and inter-protein buried surface areas. This information supports the calculation of electrostatic and hydrophobic interaction energies and also makes it possible to explore more fine-grained (e.g., atomistic) modeling approaches for studying the mechanisms of Gag polymerization and assembly.

In summary, the differential-equation literature on Gag has produced well-tested descriptions of each individual stage, and Table 1 shows how much of the underlying biochemistry is already captured in quantitative form. The next step is to connect these descriptions. The couplings are already present in the published equations, as boundary terms and source terms that were held constant for convenience. Making them dynamic, spatially resolved, and thermodynamically consistent is the central modelling problem of the next few years. It is also the problem most likely to yield antiviral targets that act on the assembly pathway as a whole rather than on a single reaction within it.

Author Contributions: Writing—original draft preparation, Q.T.; writing—review and editing, Q.T., J.Y., Y.P. and Y.L.; funding acquisition, Y.L. All authors have read and agreed to the published version of the manuscript.

Funding: This research was funded by a grant from the National Natural Science Foundation of China, grant number 12371487.

Institutional Review Board Statement: Not applicable.

Informed Consent Statement: Not applicable.

Data Availability Statement: No new data were created or analyzed in this study. Data sharing is not applicable to this article.

Acknowledgments: During the preparation of this manuscript, the authors used DeepSeek-V4-Flash for the purposes of language polishing. The authors have reviewed and edited the output and take full responsibility for the content of this publication.

Conflicts of Interest: The authors declare no conflicts of interest.

Abbreviations

The following abbreviations are used in this manuscript:

HIV-1	Human immunodeficiency virus type 1
AIDS	Acquired immunodeficiency syndrome
UNAIDS	Joint United Nations Programme on HIV/AIDS
MA	Matrix
CA	Capsid
SP1	Spacer peptide 1
NC	Nucleocapsid
SP2	Spacer peptide 2

References

1. Douek, D.C.; Roederer, M.; Koup, R.A. Emerging Concepts in the Immunopathogenesis of AIDS. *Annu. Rev. Med.* **2009**, *60*, 471–484. [CrossRef] [PubMed]

2. Barré-Sinoussi, F.; Chermann, J.C.; Rey, F.; Nugeyre, M.T.; Chamaret, S.; Gruest, J.; Dauguet, C.; Axler-Blin, C.; Vézinet-Brun, F.; Rouzioux, C.; et al. Isolation of a T-lymphotropic retrovirus from a patient at risk for acquired immune deficiency syndrome (AIDS). *Science* **1983**, *220*, 868–871. [CrossRef] [PubMed]
3. Freed, E.O. HIV-1 assembly, release and maturation. *Nat. Rev. Microbiol.* **2015**, *13*, 484–496. [CrossRef] [PubMed]
4. Sundquist, W.I.; Krusslich, H.G. HIV-1 Assembly, Budding, and Maturation. *Cold Spring Harb. Perspect. Med.* **2012**, *2*, a006924. [CrossRef] [PubMed]
5. Martinez, N.W.; Xue, X.; Berro, R.G.; Kreitzer, G.; Resh, M.D. Kinesin KIF4 regulates intracellular trafficking and stability of the human immunodeficiency virus type 1 Gag polyprotein. *J. Virol.* **2008**, *82*, 9937–9950. [CrossRef] [PubMed]
6. Sumner, C.; Ono, A. The "basics" of HIV-1 assembly. *PLoS Pathog.* **2024**, *20*, e1011937. [CrossRef] [PubMed]
7. Ono, A. HIV-1 Assembly at the Plasma Membrane: Gag Trafficking and Localization. *Future Virol.* **2009**, *4*, 241–257. [CrossRef] [PubMed]
8. Liu, Y.; Zou, X. A new model system for exploring assembly mechanisms of the HIV-1 immature capsid in vivo. *Bull. Math. Biol.* **2019**, *81*, 1506–1526. [CrossRef] [PubMed]
9. Lee, S.K.; Potempa, M.; Swanstrom, R. The choreography of HIV-1 proteolytic processing and virion assembly. *J. Biol. Chem.* **2012**, *287*, 40867–40874. [CrossRef] [PubMed]
10. Kleinpeter, A.B.; Freed, E.O. Mechanisms of HIV-1 assembly, release and maturation. *Nat. Rev. Microbiol.* **2026**, *24*, 685–701. [CrossRef] [PubMed]
11. Li, F.; Goila-Gaur, R.; Salzwedel, K.; Kilgore, N.R.; Reddick, M.; Matallana, C.; Castillo, A.; Zoumplis, D.; Martin, D.E.; Orenstein, J.M.; et al. PA-457: A potent HIV inhibitor that disrupts core condensation by targeting a late step in Gag processing. *Proc. Natl. Acad. Sci. USA* **2003**, *100*, 13555–13560. [CrossRef] [PubMed]
12. Nowicka-Sans, B.; Protack, T.; Lin, Z.; Li, Z.; Zhang, S.; Sun, Y.; Samanta, H.; Terry, B.; Liu, Z.; Chen, Y.; et al. Identification and Characterization of BMS-955176, a Second-Generation HIV-1 Maturation Inhibitor with Improved Potency, Antiviral Spectrum, and Gag Polymorphic Coverage. *Antimicrob. Agents Chemother.* **2016**, *60*, 3956–3969. [CrossRef] [PubMed]
13. Kelly, B.N.; Kyere, S.; Kinde, I.; Tang, C.; Howard, B.R.; Robinson, H.; Sundquist, W.I.; Summers, M.F.; Hill, C.P. Structure of the Antiviral Assembly Inhibitor CAP-1 Complex with the HIV-1 CA Protein. *J. Mol. Biol.* **2007**, *373*, 355–366. [CrossRef] [PubMed]
14. Blair, W.S.; Pickford, C.; Irving, S.L.; Brown, D.G.; Anderson, M.; Bazin, R.; Cao, J.; Ciaramella, G.; Isaacson, J.; Jackson, L.; et al. HIV Capsid is a Tractable Target for Small Molecule Therapeutic Intervention. *PLoS Pathog.* **2010**, *6*, e1001220. [CrossRef] [PubMed]
15. Segal-Maurer, S.; DeJesus, E.; Stellbrink, H.-J.; Castagna, A.; Richmond, G.J.; Sinclair, G.I.; Siripassorn, K.; Ruane, P.J.; Berhe, M.; Wang, H.; et al. Capsid Inhibition with Lenacapavir in Multidrug-Resistant HIV-1 Infection. *N. Engl. J. Med.* **2022**, *386*, 1793–1803. [CrossRef] [PubMed]
16. Perlmutter, J.D.; Hagan, M.F. Mechanisms of virus assembly. *Annu. Rev. Phys. Chem.* **2015**, *66*, 217–239. [CrossRef] [PubMed]
17. Liu, J.; Munoz-Alicea, R.; Huang, T.; Tavener, S.; Chen, C. A Mathematical Model for Intracellular HIV-1 Gag Protein Transport and its Parallel Numerical Simulations. *Procedia Comput. Sci.* **2012**, *9*, 679–688. [CrossRef]
18. Wang, Y.W.; Tan, J.Y.; Farrah, S.M.; Liu, J.; Zou, X. Mathematical modeling for intracellular transport and binding of HIV-1 Gag proteins. *Math. Biosci.* **2015**, *262*, 198–205. [CrossRef] [PubMed]
19. Liu, Y.; Zou, X. Mathematical modeling and quantitative analysis of HIV-1 Gag trafficking and polymerization. *PLoS Comput. Biol.* **2017**, *13*, e1005733. [CrossRef] [PubMed]
20. Endres, D.; Zlotnick, A. Model-based analysis of assembly kinetics for virus capsids or other spherical polymers. *Biophys. J.* **2002**, *83*, 1217–1230. [CrossRef] [PubMed]
21. Munoz-Alicea, R. HIV-1 Gag Trafficking and Assembly: Mathematical Models and Numerical Simulations. Doctoral Dissertation, Colorado State University, Fort Collins, CO, USA, 2013.
22. Sadre-Marandi, F.; Liu, Y.; Liu, J.; Tavener, S.; Zou, X. Modeling HIV-1 viral capsid nucleation by dynamical systems. *Math. Biosci.* **2015**, *270*, 95–105. [CrossRef] [PubMed]
23. Liu, Y.; Zeng, M.; Liu, S.; Li, C. Dynamics analysis of building block synthesis reactions for virus assembly in vitro. *Math. Biosci. Eng.* **2022**, *20*, 4082–4102. [CrossRef] [PubMed]
24. Liu, Y.; Peng, Y. Mathematical analysis of synthesis chemical reactions for virus building block polymers in vivo. *Math. Biosci. Eng.* **2024**, *21*, 6393–6406. [CrossRef] [PubMed]
25. Liu, Y.; Zou, X. Mathematical modeling of HIV-like particle assembly in vitro. *Math. Biosci.* **2017**, *288*, 46–51. [CrossRef] [PubMed]
26. Zlotnick, A. To build a virus capsid. An equilibrium model of the self-assembly of polyhedral protein complexes. *J. Mol. Biol.* **1994**, *241*, 59–67. [PubMed]
27. Hagan, M.F.; Elrad, O.M. Understanding the Concentration Dependence of Viral Capsid Assembly Kinetics-the Origin of the Lag Time and Identifying the Critical Nucleus Size. *Biophys. J.* **2009**, *98*, 1065–1074. [CrossRef] [PubMed]
28. Lei, J. *Systems Biology, Modeling, Analysis, and Simulation*; Springer: Berlin/Heidelberg, Germany, 2021.

29. Ayton, G.S.; Voth, G.A. Multiscale Computer Simulation of the Immature HIV-1 Virion. *Biophys. J.* **2010**, *99*, 2757–2765. [CrossRef] [PubMed]
30. Grime, J.M.A.; Dama, J.F.; Ganser-Pornillos, B.K.; Woodward, C.L.; Jensen, G.J.; Yeager, M.; Voth, G.A. Coarse-grained simulation reveals key features of HIV-1 capsid self-assembly. *Nat. Commun.* **2016**, *7*, 11568–11579. [CrossRef] [PubMed]
31. Dharmavaram, S.; She, S.B.; Lázaro, G.; Hagan, M.F.; Bruinsma, R. Gaussian curvature and the budding kinetics of enveloped viruses. *PLoS Comput. Biol.* **2019**, *15*, e1006602. [CrossRef] [PubMed]
32. Stewart, M.P.; Helenius, J.; Toyoda, Y.; Ramanathan, S.P.; Muller, D.J.; Hyman, A.A. Hydrostatic pressure and the actomyosin cortex drive mitotic cell rounding. *Nature* **2011**, *469*, 226–230. [CrossRef] [PubMed]
33. Nermut, M.V.; Zhang, W.H.; Francis, G.; Čiampor, F.; Morikawad, Y.; Jones, I.M. Time course of gag protein assembly in HIV-1-infected cells: A study by immunoelectron microscopy. *Virology* **2003**, *305*, 219–227. [CrossRef] [PubMed]
34. Resh, M.D. A myristoyl switch regulates membrane binding of HIV-1 Gag. *Proc. Natl. Acad. Sci. USA* **2004**, *101*, 417–418. [CrossRef] [PubMed]
35. Kutluay, S.B.; Bieniasz, P.D. Analysis of the initiating events in HIV-1 particle assembly and genome pack-aging. *PLoS Pathog.* **2010**, *6*, e1001200. [CrossRef] [PubMed]
36. Pornillos, O.; Ganser-Pornillos, B.K.; Kelly, B.N.; Hua, Y.; Whitby, F.G.; Stout, C.D.; Sundquist, W.I.; Hill, C.P.; Yeager, M. X-Ray Structures of the Hexameric Building Block of the HIV Capsid. *Cell* **2009**, *137*, 1282–1292. [CrossRef] [PubMed]
37. Pornillos, O.; Ganser-Pornillos, B.K.; Banumathi, S.; Hua, Y.; Yeager, M. Disulfide Bond Stabilization of the Hexameric Capsomer of Human Immunodeficiency Virus. *J. Mol. Biol.* **2010**, *401*, 985–995. [CrossRef] [PubMed]
38. Klipp, E.; Herwig, R.; Kowald, A.; Wierling, C.; Lehrach, H. *Systems Biology in Practice, Concepts, Implementation and Application*; WILEY-VCH Verlag GmbH & Co. KGA: Weinheim, Germany, 2008.
39. Jouvenet, N.; Neil, S.; Bess, C.; Johnson, M.C.; Virgen, C.A.; Simon, S.M.; Bieniasz, P.D. Plasma membrane is the site of productive HIV-1 particle assembly. *PLoS Biol.* **2006**, *4*, 2296–2310. [CrossRef] [PubMed]
40. Datta, S.; Zhao, Z.; Clark, P. Interactions between HIV-1 Gag molecules in solutions: An inositol phosphate-mediated switch. *J. Mol. Biol.* **2007**, *19*, 799–811. [CrossRef] [PubMed]
41. Campbell, S.; Rein, A. In vitro assembly properties of human immunodeficiency virus type 1 Gag protein lacking the p6 domain. *J. Virol.* **1999**, *73*, 2270–2279. [CrossRef] [PubMed]
42. Jouvenet, N.; Bieniasz, P.D.; Simon, S.M. Imaging the biogenesis of individual HIV-1 virions in live cells. *Nature* **2008**, *454*, 236. [CrossRef] [PubMed]
43. Surhone, L.M.; Timpledon, M.T.; Marseken, S.F. *Regularization (Mathematics)*; Betascript Publishing: Beau Bassin, Mauritius, 2010.
44. Woodward, C.L.; Cheng, S.N.; Jensen, G.J. Electron cryotomography studies of maturing HIV-1 particles reveal the assembly pathway of the viral core. *J. Virol.* **2015**, *89*, 1267–1277. [CrossRef] [PubMed]
45. Frank, G.A.; Narayan, K.; Bess, J.W., Jr.; Del Prete, G.Q.; Wu, X.; Moran, A.; Hartnell, L.M.; Earl, L.A.; Lifson, J.D.; Subramaniam, S. Maturation of the HIV-1 core by a non-diffusional phase transition. *Nat. Commun.* **2015**, *6*, 5854. [CrossRef] [PubMed]
46. Ning, J.; Erdemci-Tandogan, G.; Yufenyuy, E.L.; Wagner, J.; Himes, B.A.; Zhao, G.; Aiken, C.; Zandi, R.; Zhang, P. In vitro protease cleavage and computer simulations reveal the HIV-1 capsid maturation pathway. *Nat. Commun.* **2016**, *7*, 13689. [CrossRef] [PubMed]
47. Miczi, M.; Diós, Á.; Bozóki, B.; Tőzsér, J.; Mótyán, J.A. Development of a bio-layer interferometry-based protease assay using HIV-1 protease as a model. *Viruses* **2021**, *13*, 1183. [CrossRef] [PubMed]
48. Laco, G.S. HIV-1 Gag Non-Cleavage Site PI Resistance Mutations Stabilize Protease/Gag Substrate Complexes in Silico via a Substrate-Clamp. *Biochemistry* **2021**, *1*, 190–209. [CrossRef]
49. Johnson, G.T.; Goodsell, D.S.; Autin, L.; Forli, S.; Sanner, M.F.; Olson, A.J. 3D molecular models of whole HIV-1 virions generated with cellPACK. *Faraday Discuss.* **2014**, *169*, 23–44. [CrossRef] [PubMed]

Disclaimer/Publisher's Note: The statements, opinions and data contained in all publications are solely those of the individual author(s) and contributor(s) and not of MDPI and/or the editor(s). MDPI and/or the editor(s) disclaim responsibility for any injury to people or property resulting from any ideas, methods, instructions or products referred to in the content.